Creative Education, 2025, 16(10), 1680-1687
https://www.scirp.org/journal/ce
ISSN Online: 2151-4771
ISSN Print: 2151-4755

All-Optical, Qualitative Diamond Magnetometry

Arius Seow[1], Luna Xu[2]

[1]Princeton Day School, Princeton, NJ, USA
[2]Princeton High School, Princeton, NJ, USA
Email: ariusseow@gmail.com, lunaxunj@gmail.com

How to cite this paper: Seow, A., & Xu, L. N. (2025). All-Optical, Qualitative Diamond Magnetometry. *Creative Education, 16,* 1680-1687.
https://doi.org/10.4236/ce.2025.1610103

Received: August 9, 2025
Accepted: October 24, 2025
Published: October 27, 2025

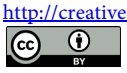

Abstract

The nitrogen-vacancy center in diamond offers unique possibilities for room-temperature quantum magnetometry. Here, we demonstrate and explore diamond magnetometry with a portable, educational toolkit from Quantum Education Initiative (QEI). A green (532 nm) laser diode and optical elements are used to electronically excite NV^- electrons, while a transverse magnetic field induces spin mixing. Through all-optical initialization and readout (fluorescence), we gained a conceptual understanding of diamond-based magnetometry. We aligned several optical elements and measured intensity data to create an intensity versus magnetic field relationship. The employed magnetometry scheme does not attain state of the art sensitivities, but it is purely employed for educational purposes.

Keywords

NV Center, Diamond Magnetometry, Photoluminescence, Education

1. Introduction

Magnetometry, the science of measuring magnetic fields, plays a critical role in a wide range of scientific and technological applications (Lu, Zhao, Zhu, Liu, Zhuang, Fang, & Zhang, 2023). From mapping the Earth's geomagnetic field and detecting hidden archaeological structures to guiding navigation systems and probing fundamental properties of materials, magnetometers serve as indispensable tools across disciplines (Lu, Zhao, Zhu, Liu, Zhuang, Fang, & Zhang, 2023). Conventional magnetometers, such as fluxgate, Hall-effect, and superconducting quantum interference devices (SQUIDs), have long been used to detect and quantify magnetic fields with varying degrees of sensitivity, spatial resolution, and operating conditions (Hrvoic, Hollyer, & Eng, 2005). However, many of these traditional methods require cryogenic temperatures, bulky components, or exhibit limited bandwidth and dynamic range (Hrvoic, Hollyer, & Eng, 2005). Recent ad-

vances in quantum technology have introduced new paradigms for magnetic field detection, particularly through solid-state spin systems. Among these, the nitrogen-vacancy (NV) center in diamond has emerged as a robust platform for magnetometry. Unlike many high-precision sensors that demand complex infrastructure, NV-based magnetometers operate at room temperature, offer high spatial resolution, and are compatible with optical interrogation techniques (Hong, Grinolds, Pham, Le Sage, Luan, Walsworth, & Yacoby, 2013). These properties have made them especially attractive not only for cutting-edge research but also for educational settings seeking to make quantum sensing concepts more accessible. Magnetometers based on the negatively charged nitrogen-vacancy (NV^-) center are distinctive because the same optical beam can both polarize and read out the electron spin at room temperature. Under green excitation, spin-dependent intersystem crossing preferentially pumps population into the ms = 0 m_s = 0 ms = 0 sublevel of the spin-1 ground state, which fluoresces more brightly than ms = ±1 m_s = \pm 1 ms = ±1. As a result, small perturbations that redistribute spin populations—most notably magnetic fields—translate into measurable changes in red PL, enabling optically detected magnetometry without cryogenics or vacuum hardware (Rondin, 2014).

The nitrogen-vacancy (NV) center in diamond is a point defect comprising a substitutional nitrogen atom adjacent to a vacant lattice site (Rondin, 2014). This defect can exist in various charge states—neutral (NV^0), negatively charged (NV^-), or positively charged (NV^+)—depending on the local electrostatic environment (Rondin, 2014). While both NV^0 and NV^- exhibit photoluminescence (PL), only the NV^- charge state possesses a spin-1 (triplet) ground state that can be optically initialized, coherently manipulated, and read out via spin-dependent fluorescence (Rondin, 2014). The neutral NV^0 and positive NV^+ charge states are not suitable for all-optical magnetometry: NV^0 has a spin-1/2 ground state with negligible spin-dependent intersystem crossing at room temperature, yielding little fluorescence (PL) contrast, while NV^+ is effectively non-fluorescent and lacks an accessible electron-spin manifold; by contrast, NV^- has a spin-1 triplet ground state with strong spin-selective decay, enabling transverse-field–induced spin mixing to be read out as PL changes. Crucially, the NV^- spin Hamiltonian is linearly sensitive to the projection of an external magnetic field along the NV axis, enabling precise magnetic field detection through Zeeman-induced shifts in the spin sublevels (Rondin, 2014). Conventional NV magnetometry relies on microwave-driven electron spin resonance (ESR) to resolve these shifts; however, in this work, we implement a simplified, all-optical approach suitable for educational settings (Rondin, 2014; Lopez, 2015). In the presence of a magnetic field, the spin sublevels ms = ±1 experience opposite Zeeman shifts of ±μgB, leading to a redistribution of spin populations that affects the overall fluorescence intensity (Rondin, 2014; Lopez, 2015). Under continuous 532 nm excitation, NV^- centers cycle between a spin-triplet ground state, a spin-triplet excited state, and intermediate singlet "shelving" states. The intersystem crossing rate is higher for $m_s = \pm 1$ than $m_s = 0$, so optical pumping accumulates population in $m_s = 0$ state, yielding higher PL. A

magnetic field parallel to the NV axis splits the non-zero magnetic spin states but preserves spin purity; a field transverse to the axis mixes $m_s = 0$ and $m_s = \pm 1$, partially defeating optical pumping and decreasing PL (Rondin, 2014). In the vicinity of LACs, mixing is greatly enhanced, which steepens the PL response to small field changes (Rondin, 2014; Lopez, 2015). Both lowering noise (e.g., by shielding ambient light) and increasing slope (e.g., by working near an LAC) can improve performance without microwaves. Although this method does not resolve resonance frequencies directly, changes in photoluminescence intensity under varying transverse magnetic fields can serve as a qualitative proxy for magnetic field strength. This behavior, consistent with prior studies, forms the basis for our accessible, resonance-free magnetometry demonstration. Beyond a laboratory curiosity, NV-diamond magnetometry underpins real-world sensing across biomedicine, navigation, geoscience, and microelectronics. In biomedicine, chip-scale NV sensors are being explored for label-free detection of magnetic nanoparticles, microscale current mapping in neurons and cardiac tissue, and benchtop NMR/MRI at modest fields, promising portable assays without cryogenics. In navigation and geophysics, compact NV instruments can support magnetic-anomaly navigation in GPS-denied settings, rapid UXO/archaeology surveys, and geomagnetic field mapping with high spatial resolution and wide dynamic range. In microelectronics and energy systems, NV imaging enables non-invasive current-density mapping, failure analysis of integrated circuits, and visualization of vortices in superconductors and spin textures in magnetic materials, while also diagnosing stray fields and eddy currents in motors, transformers, and battery packs.

For students, this platform matters because it connects abstract quantum concepts to tangible measurements with a safe, room-temperature, and low-overhead setup. A single apparatus teaches optical alignment, noise budgeting, background subtraction, and uncertainty analysis; it also scaffolds core ideas—spin polarization, Zeeman shifts, and spin mixing—into practical data products (contrast, sensitivity, and calibration curves). The activity naturally scales: starting from PL-versus-field trends (as in this work), cohorts can progress to ODMR for absolute field readout, vector magnetometry using multiple NV orientations, lock-in detection for sensitivity gains, and eventually magnetic imaging or microscale NMR. Pedagogically, NV magnetometry is a cross-disciplinary gateway that builds the quantum workforce skill set (experimental design, electronics, optics, coding, and modeling) while remaining budget-conscious and reproducible. By linking the physics of a point defect in diamond to applications students recognize—medical diagnostics, navigation, and chip reliability—the module motivates deeper study and equips learners with techniques directly transferable to research and industry.

While all-optical diamond magnetometry has been demonstrated (as shown above), the scope of the toolkit covers solely the qualitative relationship between the magnitude of a transverse field and the integrated photoluminescence intensity. **Figure 1** was employed as a model to give us an expectation for how an increasing amplitude magnetic field can lead to a decreasing fluorescence. It is important to note the model data was taken near a level anticrossing, significantly

increasing sensitivity to the field (Lopez, 2015).

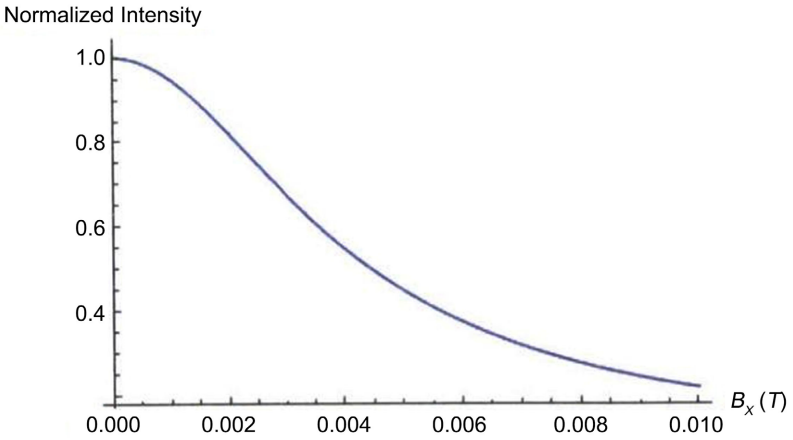

Figure 1. Photoluminesence intensity versus transverse magnetic field. Adapted from (Lopez, 2015).

2. Methodology

QEI's toolkit and associated manual were followed for the methodology. The toolkit consisted of a LaserLand 532 nm green laser line projector module, a ThorLabs PDA36A2 Si switchable gain detector, a ThorLabs RMS40X Olympus plan achromat objective, a ThorLabs RMS10x Olympus plan achromat objective, a ThorLabs DMLP567 long pass dichroic mirror, a Commercial Electric Auto-Ranging Multimeter, and QEI's optical breadboards and posts. First, we observed safety protocols using laser safety glasses of optical density (OD) 5 (for 532 nm light). The glasses transmitted a negligible amount of green light, while still allowing enough room light to conduct the experiment. Next, the fluorescence microscope was aligned. The 532 nm diode provides continuous-wave excitation that is reflected by a long-pass dichroic (cut-on at ~567 nm) into a 40×, NA 0.65 dry objective to focus on the NV layer; the same objective collects red PL, which passes the dichroic mirror before being refocused by a 10×, NA 0.25 objective onto the silicon photodiode. This arrangement ensures efficient green delivery and red collection while suppressing residual pump light at the detector (**Figure 2**).

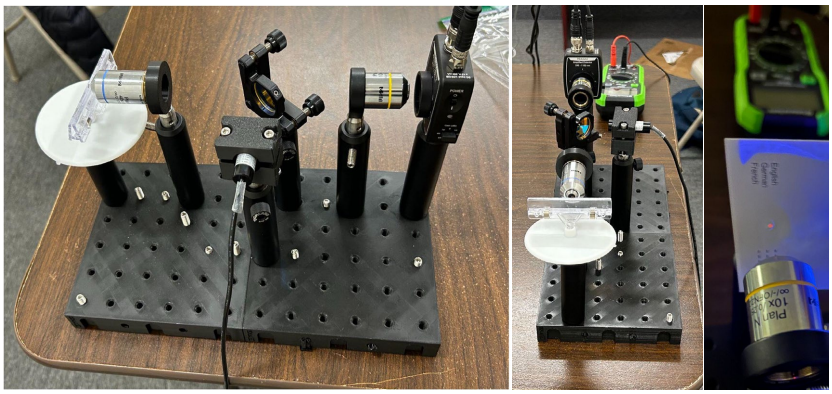

Figure 2. Fluorescence microscope setup (left and middle), with focused fluorescence (right).

The laser (532 nanometer laser diode) was aligned to reflect at approximately 45 degrees with respect to a dichroic mirror. The reflected light was focused via a dry microscope objective (40x, 0.65 NA) onto an NV diamond plate. The fluorescence was also collected and collimated by the same objective. The only specification provided for the diamond plate was the NV concentration of 3 parts per million. Another objective (10x, 0.25 NA) was aligned to the photodetector with a bandpass filter such that photons with a wavelength greater than 580 nm were transmitted and focused onto the detector. We also switched the positions of the two microscope objectives and observed the importance of a high numerical aperture for focusing green light and collecting red light from the diamond. A handheld multimeter was connected to the photodetector via a banana to coaxial cable. The detector's x, y, and z position were optimized first using a post-it (to approximate the focal point) and next by maximizing the voltage relayed by the multimeter. Furthermore, by observing the light reflected on the wall (far-field), we corrected for obvious skewness or misalignment of the laser. Since a free-space photodetector was used for readout, background counts from the detector were measured at each gain level (in the presence of room light):

Gain (dB)	Voltage (mV)
0	0.4
10	3.7
20	5.9
30	8.3
40	11.2
50	13.7
60	15.83

It is important to note that the intensity of room light may not be constant at all times, revealing a source of error in our data. While turning off the room light would increase our signal to noise ratio, we were unable to clearly record the voltage on the multimeter in the dark. Once the setup was optimized and the background counts were collected, three magnets were introduced. Each magnet was placed at a fixed distance from the diamond. The fluorescence intensity was measured three times over a period of 4 minutes. We used the average value as the metric to report and repeated this measurement for 4 different positions of the magnet. To approximate the distance between the magnet and diamond, the magnet was only placed on a through hole. By varying the distance between the diamond and the magnet, the field was effectively varied. We then had to decide which of the magnets had the strongest transverse component with respect to the NV ensemble used for measurements. By comparing the magnitudes of intensity measured on the photodetector for each magnet, magnet 2 was deduced to have the strongest transverse component since it yielded the lowest photoluminescence for each fixed distance. The "transverse" may be defined with respect to the NV

symmetry axis of the ensemble (approximated here by the surface normal of the diamond plate). For each magnet at a fixed distance, we rotated the magnet in the plane of the diamond while monitoring the photoluminescence intensity; the orientation that produced the minimum PL was assumed to correspond to the largest transverse field (maximal spin mixing). That orientation was then fixed for data collection at different distances (Tables 1-3).

Table 1. Distance versus photoluminescence for magnet 1.

Distance (inches)	PL (t = 1 min) (mV)	PL (t = 2 min) (mV)	PL (t = 4 min) (mV)
1"	59.2	60.7	60.4
1.4"	60.1	59.8	59.7
2	62.9	63.2	62.4
Infinity	64.1	63.5	63.8

Table 2. Distance versus photoluminescence for magnet 2.

Distance (inches)	PL (t = 1 min) (mV)	PL (t = 2 min) (mV)	PL (t = 4 min) (mV)
1"	63.1	62.9	63.4
1.4"	63.3	61.8	62.7
2	63.3	62.9	63.3
Infinity	63.3	64.2	63.7

Table 3. Distance versus photoluminescence for magnet 3.

Distance (inches)	PL (t = 1 min) (mV)	PL (t = 2 min) (mV)	PL (t = 4 min) (mV)
1"	62.6	62.7	62.9
1.4"	63.1	62.8	62.7
2	63.3	62.9	63.3
Infinity	63.6	64.2	63.9

3. Results

Using the through holes, on which all components are mounted, the relative distance from the diamond can be approximated. The distance between two collinear, adjacent screw holes is 1 inch; the distance between two adjacent, diagonal screw holes is thus approximated as 1.4 inches. The photoluminescence was recorded for each magnet-distance pair via the voltage reported on the multimeter. A fixed gain of 50 dB was used for all table data. The distance of infinity was approximated by removing the magnet from the setup. As expected, the photoluminescence values for all magnets at an infinite distance are about the same. Since the average difference in photoluminescence between when the diamond was placed at an infinite distance away and 1" away is largest for magnet 1, we conclude that magnet 1 must have the strongest transverse field component. It is important to note the differences in voltage recorded for the same magnet-distance

pair across time, portraying the effect of noise. The signal to noise ratio as defined by the ratio of the voltage when the diamond is aligned with the diamond not aligned. Since the voltage on the photodetector from just the room light at 50 dB was 13.7 mV, we approximate our SNR to be 63.81

$$\frac{63.81-13.7}{13.7}=3.66.$$

Although we did not calibrate the absolute magnetic field, the contrast values provide a path to calibration. If one independently measures BBB at each distance with a Hall probe (or performs a one-time ODMR measurement to translate a Zeeman shift into field), the same PL data could be fit to an empirical I(B)I(B)I(B) curve. A simple dipole-field model for the magnet—while approximate—would then allow interpolation of BBB for unmeasured positions.

From an educational standpoint, the exercise emphasizes three transferable skills: 1) Building a repeatable optical alignment protocol with quantitative criteria (voltage peaking, gain linearity); 2) Designing a data-collection plan that separates random noise from systematic drift (triplicate measurements over minutes); 3) Reporting uncertainty with transparent background corrections. These habits map directly onto advanced NV experiments (e.g., ODMR vector magnetometry) and onto other optical sensing modalities.

4. Conclusion

This work demonstrates the feasibility of QEI's all-optical, diamond magnetometry toolkit. By employing a trivial measurement protocol, we were able to align optical components, collect fluorescence data, and qualitatively assess magnetic field strength through photoluminescence contrast. While we did not explore quantum magnetometry, we gained hands-on experience with fluorescence microscopy and how transverse magnetic fields can affect the NV fluorescence via spin mixing. We measured the NV photoluminescence across different magnets and their distance from the diamond to qualitatively assess the relationship between magnetic field and photoluminescence intensity, ultimately identifying which magnet had the strongest transverse field. Thus, the measurements were not taken near the LAC regions with high sensitivity to transverse fields, highlighting the main performance limitation of this magnetometry setup. A level anticrossing (LAC) is a magnetic-field region where NV^- spin sublevels hybridize, which enhances spin mixing and the spin-dependent PL contrast. Operating near an LAC steepens the slope of the change in photoluminescence intensity with respect to the magnetic field, so small field changes produce larger PL changes, yielding higher sensitivity than the off-LAC measurements used here. Ultimately, the setup provided a hands-on learning experience for understanding quantum magnetometry with a fascinating piece of diamond.

Looking ahead, three incremental upgrades would transform this qualitative exercise into a quantitative laboratory: 1) Enclose the detection path and add lock-in detection to suppress ambient-light noise; 2) Incorporate a simple field calibra-

tion (Hall probe or a brief ODMR scan) to convert PL changes into ΔB. These changes preserve the portability and low cost of the QEI toolkit while enabling sensitivity improvements and richer analyses (e.g., contrast-versus-power curves, Allan deviation) appropriate for advanced undergraduate or early graduate curricula.

Conflicts of Interest

The authors declare no conflicts of interest regarding the publication of this paper.

References

Hong, S., Grinolds, M. S., Pham, L. M., Le Sage, D., Luan, L., Walsworth, R. L. et al. (2013). Nanoscale Magnetometry with NV Centers in Diamond. *MRS Bulletin, 38,* 155-161. https://doi.org/10.1557/mrs.2013.23

Hrvoic, I., Hollyer, G. M., & Eng, P. (2005). Brief Review of Quantum Magnetometers. *GEM Systems.*

Lopez, N. A. (2015). *All-Optical Method of Nanoscale Magnetometry for Ensembles of Nitrogen-Vacancy Defects in Diamond.* Massachusetts Institute of Technology.

Lu, Y., Zhao, T., Zhu, W., Liu, L., Zhuang, X., Fang, G. et al. (2023). Recent Progress of Atomic Magnetometers for Geomagnetic Applications. *Sensors, 23,* Article 5318. https://doi.org/10.3390/s23115318

Rondin, L., Tetienne, J., Hingant, T., Roch, J., Maletinsky, P., & Jacques, V. (2014). Magnetometry with Nitrogen-Vacancy Defects in Diamond. *Reports on Progress in Physics, 77,* Article 056503. https://doi.org/10.1088/0034-4885/77/5/056503